# Title: Thermo-mechanical pressurization of experimental faults in cohesive rocks during seismic slip

**Authors:** Violay, M.[1,2*], Di Toro, G.[3,4], Nielsen, S.[5], Spagnuolo, E.[6], Burg, J.P.[1]

**Affiliations:**

[1] ETH D-ERDW, Sonnegstrasse, 5 CH-8092, Zürich, Switzerland

[2]EPFL-ENAC, LEMR, Station 18 CH-1015, Lausanne, Switzerland

[3] Dipartimento di Geoscienze, Università degli Studi di Padova, Via G. Gradenigo 6, 35131, Padua, Italy

[4] School of Earth, Atmospheric & Environmental Sciences, University of Manchester, Oxford Road, Manchester M13 9PL, UK

[5] Earth Sciences Department, University of Durham, South Road, Durham DH13LE, UK

[6] Instituto Nazionale di Geofisica e Vulcanologia, Via di Vigna Murata 605, 00143, Rome, Italy

**Correspondence to:** *marie.violay@epfl.ch*

## Highlights:

High velocity friction experiments on cohesive rocks under undrained conditions

Experimental evidence of thermo-mechanical pressurization (TMP)

TMP weakening of cohesive rocks is negligible during earthquakes

## Keywords:

Friction, earthquakes, fluids, thermo-mechanical pressurization, basalt, marble

## Abstract:

Earthquakes occur because fault friction weakens with increasing slip and slip rates. Since the slipping zones of faults are often fluid-saturated, thermo-mechanical pressurization of pore fluids has been invoked as a mechanism responsible for frictional dynamic weakening, but experimental evidence is lacking. We performed friction experiments (normal stress 25 MPa, maximal slip-rate ~3 ms$^{-1}$) on cohesive basalt and marble under (1) room-humidity and (2) immersed in liquid water (drained and undrained) conditions. In both rock types and independently of the presence of fluids, up to 80% of frictional weakening was measured in the first 5 cm of slip. Modest pressurization-related weakening appears only at later stages of slip. Thermo-mechanical pressurization weakening of cohesive rocks can be negligible during earthquakes due to the triggering of more efficient fault lubrication mechanisms (flash heating, frictional melting, etc.).

## Introduction

During earthquakes, few millimeters thick slip zones within fluid-saturated, cohesive or non-cohesive rocks are sheared over several meters (80 m for the Tohoku 2011 Mw 9.0 earthquake, **Fujiwara et al., 2011**) at slip rates of meters per second and under normal stresses up to hundreds of MPa (**Sibson, 1973; Rice, 2006**). The frictional power per unit area (product of the slip rate per frictional shear stress, in the range of 1-100 MW m$^{-2}$) is dissipated as heat and rock fragmentation in the slipping zone (**Sibson, 1980**). This large power triggers several mechano-chemical processes that may induce frictional weakening (**Di Toro et al., 2011; Goldsby and Tullis, 2011; Reches and Lockner, 2010**). Thermo-mechanical pressurization (TMP) of pore fluids trapped is one of the possible processes responsible for fault dynamic weakening (**Sibson, 1973; Rice,1992; 2006; Lachenbruch, 1980; Brantut et al., 2010; Bizzari and Cocco, 2006; Segall and Rice, 2008; Wibberley and Shimamoto, 2005**). Given the widespread presence of fluids in natural slipping zones, TMP has been thoroughly investigated from a theoretical point of view. TMP models are based on two competing processes: fluid and rock expansion in response to shear heating and the fluid storage capacity of the rock (**Rice, 2006; Segall and Rice, 2008; Platt et al., 2014**).

Several experimental studies were carried on to investigate TMP (**Mizoguchi et al., 2009; Brantut et al., 2008; Ferri et al., 2010; 2011; De Paola et al., 2011; Mitchell et al., 2015; Faulkner et al., 2011; Ujiie et al., 2011; 2013)**. Experiments approached seismic deformation conditions by imposing slip rates (*V*) of ~1 $ms^{-1}$, slip ($\delta$) up to tens of meters, and effective normal stresses ($\sigma_n^{eff}$) of tens of MPa on clay-, calcite- and dolomite-rich gouges under room-humidity and wet conditions. The measured large weakening (up to 80-90% of friction drop at 1 $ms^{-1}$) was attributed to: (1) in part (< 20%) thermochemical pressurization associated to the breakdown of clays and release of $H_2O$ (**Brantut et al., 2008; 2010; Ferri et al., 2010**) or to the breakdown of calcite and dolomite and release of $CO_2$ (**De Paola et al., 2011; Mitchell et al., 2015**) in the case of room-humidity experiments and, (2) thermal pressurization in the case of wet experiments on clay-rich gouges (**Faulkner et al., 2011; Ferri et al., 2010; Ujiie et al., 2011; 2013**). However, technical issues related to fluid and gouge confinement impeded measuring the pore fluid pressure in the sample chamber. We installed on the rotary shear machine SHIVA (Slow-to-High-Velocity-Apparatus, INGV Rome, **Suppl. Material S1**) an on-purpose designed pressure-vessel that allows shearing cohesive rocks immersed in fluids and to measure the pore fluid pressure during the experiments (**Violay et al., 2013**). Previous experiments were performed under drained conditions on Carrara marbles and gabbros (**Violay et al., 2013; 2014**). We report new results obtained by shearing basalts and Carrara marbles under undrained conditions. Though the actual experimental configuration does not allow shearing saturated gouges, the results for cohesive rocks are intriguing: the contribution of TMP during shearing of cohesive rocks at seismic slip rates is negligible compared to the contribution from other weakening mechanisms.

**Material and methods**

To investigate seismic slip in the presence of pore fluids, 33 friction experiments (**Table 1)** were conducted at room temperature on hollow cylinders (50/30 mm external/internal diameter) of Etna basalt (Electron Micro-Probe Analysis reported in **Table 2**) and Carrara marble (99.9% calcite, X-Ray Diffraction and X-Ray Fluorescence analysis, **Violay et al., 2013**). Samples were jacketed with aluminium rings, sealed with epoxy to prevent fluid leaks and inserted in the fluid pressure vessel (**Nielsen et al., 2012**; **Suppl. Material S1**). The description of SHIVA (**Di Toro et al., 2010; Niemeijer et al., 2011**) and of the experimental configuration used to perform experiments with pressurized fluids can be found in **Suppl. Material S1**. The main difference with respect to previous studies conducted with fluids (**Violay et al., 2013; 2014**) was the disposition of the closed valves, which allowed imposing undrained conditions (see **Suppl. Material S1** for full description**)**. Experiments were performed (1) under room-humidity conditions and immersed in water, (2) drained conditions (the specimen is saturated and continuously connected to the water reservoir, (**Paterson and Wong, 2005)**, resulting in constant fluid pressure and preventing fluid pressurization) and (3) undrained conditions (the specimen was first saturated and then isolated from the water reservoir: fluid pressurization was induced by reduction in pore volume, (**Paterson and Wong, 2005)** and by increase in fluid volume due to thermal expansion during shearing). A K-Type thermocouple was inserted at about 3 mm from the slip surface of the sample to measure the temperature evolution of the fluid during the experiments. The thermocouple was installed in the "stationary side" (i.e., normal stress loading column) of SHIVA.

Experiments were performed by spinning two rock cylinders at accelerations of 7.8 $ms^{-2}$, $V$ = 3 $ms^{-1}$, 4 m < $\delta$ < 8 m, normal stress ($\sigma_n$) from 15 to 35 MPa and initial fluid pressure $P_f(t_0)$= 5 MPa (**Violay et al., 2013; 2014**). Mechanical data (axial load, torque, slip, angular rotation) were acquired at a frequency up to 25 kHz. $\delta$, $V$ and shear stress ($\tau$) were determined using methods described in **Di Toro et al.** (2010), **Niemeijer et al.,** (2011) and **Tsutsumi and Shimamoto** (1997). The two rock-types were selected because are common crustal rocks and for their relatively low porosity (< 5%) and low permeability (< $10^{-17}m^2$) (e.g., **Vinciguerra et al., 2005**). The slip zones of experiments conducted on basalts could be recovered because the two rock cylinders were welded by glass due to the solidification of the frictional melt produced during shearing. The microstructures were investigated with an optical microscope and electron probe micro-analyzer (JEOL, JXA-8200 at ETH, Zurich). The chemical compositions of grains and glasses were determined on carbon-coated, polished thin sections using an Electron Probe Micro-Analyzer (EPMA) JEOL, JXA-8200 (ETH, Zurich) with a focused beam about 1 μm in diameter under accelerating voltage of 15 kV and current 15 nA. The slipping zones of experiments conducted on Carrara marble could not be recovered *in-situ* (only few dispersed remnants were found) because they consisted of non-cohesive material that was flushed away during the ejection of the fluid from the vessel after the experiment.

**Results**

*Mechanical data*

Experiments performed under identical ambient and deformation conditions resulted in systematically reproducible mechanical data for both Etna basalt and Carrara marble (**Figs. 1-4**). We present the measurements of the friction for comparison with data obtained at different initial effective normal stresses and the measurements of the shear stress for comparison of data obtained at a given imposed initial effective normal stress (all mechanical data are summarized in **Table 1**). We define the friction coefficient based on effective normal stress ($\mu = \tau / \sigma_n^{eff}(t)$ or Terzaghi's principle for $\sigma_n^{eff}(t) = \sigma_n(t) - \alpha P_f(t)$ with $\alpha$ =1, incorporating instantaneous $\sigma_n$ and $P_f$). However, since $P_f(t)$ varies during the experiment due to effect of thermal expansion, to illustrate more clearly the effect of TMP we also present the results in Fig. 4 based on the initial value of $P_f(t_0)$ alone ($\mu = \tau / \sigma_n^{eff\text{-}0}(t)$ with $\sigma_n^{eff\text{-}0}(t) = \sigma_n(t) - P_f(t_0)$).

For Etna basalt, the coefficient of friction decayed almost exponentially from a peak value $\mu_p$=0.59±0.08 at about slip initiation (i.e., 0.64±0.05 for room humidity conditions, 0.58±0.05 for drained and 0.53±0.07 for undrained conditions) to a steady-state value $\mu_{ss}$ that decreased with increasing effective normal stress (**Figs. 1 and 4**). The $\mu_{ss}$ was determined from the average value of friction coefficient ($\mu$) between 4.5 and 5.5 meters slip, except for experiment s921 where $\mu_{ss}$ was determined between 2.5 and 3.5 meters slip. The initial decay of the friction coefficient (and thus of the shear stress) was similar independently of the ambient conditions (**Fig. 3**). At $\sigma_n^{eff}(t_0)$= 20 MPa (i.e. $\sigma_n^{eff}$ *at the initiation of the experiment)*, the residual friction coefficient after 5 cm of slip ranged from $\mu_{r\_5cm}$ = 0.20-0.25 for the room humidity (s485 and s541), to $\mu_{r\_5cm}$ = 0.26-0.28 for the drained (s921 and s926) and to $\mu_{r\_5cm}$ = 0.22-0.24 for the undrained (s922, s925, s927 and s933) experiments (**Table 1**). The $\mu_{r\_5cm}$ corresponded to a percentage of friction drop with respect to $\mu_p$ (or $\%\Delta\mu = 100\ (\mu_{r\_5cm} - \mu_{ss})/(\mu_p - \mu_{ss})$) ranging from 80.2% (s485, room humidity conditions), to 56.4% (s921, drained conditions) **(Fig. 4, and Table 1)**. Given the larger $\mu_p$ in room humidity experiments, the drop in percentage of the friction coefficient in the first 5 cm of slip was slightly larger in room humidity conditions (73.06±5.24%) than in both drained (67.96±8.36%) and undrained (68.35±3.65%) conditions (**Fig. 4**).

Instead, the steady-state shear stress ($\tau_{ss,}$ was determined from the average value of shear stress between 4.5 and 5.5 meters slip, except for experiment s921 where $\tau_{ss}$ was determined between 2.5 and 3.5 meters slip) was about 20% lower under undrained than under drained and room-humidity conditions, for similar $V$, δ, and initial $\sigma_n^{eff}(t_0)$(**Figs. 2, 3, Suppl. Material S2**). For instance, at initial $\sigma_n^{eff}(t_0)$= 20 MPa, the coefficient of friction decayed from a peak value $\mu_p$ = 0.55∓0.07 (corresponding to a shear stress of 11±1.4 MPa) towards a steady-state value $\mu_{ss}$ = 0.11∓0.01 (shear stress of 2.2±0.2 MPa) under room-humidity conditions, $\mu_{ss}$ = 0.11∓0.01 (shear stress of 2.2±0.2 MPa) under drained conditions and $\mu_{ss}$ = 0.09∓0.01 (shear stress of 1.8±0.2 MPa) and under undrained conditions (**Table 1; Fig. 2**). Under undrained conditions, an overpressure $dP$ (such that $P_f = P_f(t_0) + dP$, *(with* $P_f(t_0)$ *the fluid pressure at the initiation of the experiment*) was measured with increasing slip (**Fig. 2A**) following a power law best fitted by $dP = 8.4\ (\mp 0.6)\ \delta^{0.2(\mp 0.07)}$ [MPa] (for $\sigma_n$= 25 MPa, $V$= 3 ms$^{-1}$ $P_f(t0)$=5 MPa). Overpressure $dP$ decreased immediately by ~60% after the slip was stopped (**Fig. 2A).** Conversely, $P_f$ and $\sigma_n$ did not vary under drained conditions (**Fig. 2A**). Sample shortening rate was constant and almost negligible during the first five centimetres of slip for both drained and undrained conditions (**Fig.3B**). For slip longer than 5 cm, the shortening rate was ~0.170 mm/m and ~0.089 mm/m in drained and undrained conditions, respectively **(Fig.1, Table 1).**

For Carrara marble, the friction coefficient evolved from $\mu_p$= 0.60±0.07 to $\mu_{ss}$= 0.04±0.02 **(Table 1)**. Contrary to Etna basalt, $\tau_{ss}$ and shortening rate were almost negligible and similar (~0.0001 mm/m) under room humidity, drained and undrained conditions, even if a small pore fluid overpressure ($dP$ ~1 MPa) was measured after several meters of slip under undrained conditions (**Fig. 2B**). The $\mu_{r\_5cm}$ was larger (and similar) for both undrained

(68.96±1.79%) and drained (70.44±2.58%) conditions, than under room humidity (49.85±4.39%) conditions (**Table 1; Fig. 4D**).

*Temperature measurement*

The maximum temperature measured by the thermocouple immersed in the fluid was 35 ºC for experiment s929 performed at normal stress of 25 MPa, initial fluid pressure of 5 MPa, target slip rate of 3 $ms^{-1}$ and total slip of 6 m **(Fig. 5).** The thermocouple measured the temperature evolution with time of the water in the pressure vessel due to the frictional heat generated and diffused from the slip surface. Because of heat diffusion in water, the thermal perturbation was detected with some delay with respect to the initiation of the experiment. This renders the determination of the temperature of the sliding surface a complicated task.

*Microstructures*

After the experiments and irrespective of the ambient conditions, in Etna basalt, a continuous 100-200 μm thick layer of glassy-like material separated the rock cylinders **(Fig. 6)**. Under the optical microscope, the layer was homogeneous and brown coloured in parallel-polarized light, and extinct in cross-polarized light, suggesting that the layer was made of solidified friction melt (i.e., glass). This interpretation is consistent with the observed extrusion of drops of melt during experiments performed at room-humidity conditions, and with the presence, in all experiments, of a lump of glassy-like material preserved in the inner hole of the hollow cylinders. The electron microprobe analysis showed that, independently of the environmental conditions and in all of the experiments where steady-state friction was achieved, the glass had a chemical composition almost identical to the bulk composition of the initial basalt **(Table 2).** From image analysis of FE-SEM microphotographs, the glassy-like layer of experiments performed under room-humidity contained < 1% in volume of vesicles and ~16 ± 5% in volume of lithic clasts (< 10 µm in size); instead, in experiments performed in the presence of fluids, the glassy-like layer contained 3±2% in volume of vesicles and ~9±3 % in volume of lithic clasts (< 10 µm in size) in both drained and undrained conditions **(Fig. 6).**

For Carrara marble, in room-humidity experiments performed at $\sigma_n^{eff}(t_0)$ = 20 MPa, δ= 4÷7 m and $V$ = 3 ms$^{-1}$ s, the wall rocks were separated by ~100 µm thick continuous slip zone composed of fine-grained (< 50 nm in size) non-cohesive material (see Fig. 5 in **Violay et al., 2013**). In drained and undrained experiments, the compacted gouge layers were not investigated because they could not be found on the slip zone.

**Discussion**

In the two rock types under both room-humidity and drained conditions, $\mu_p$ and $\mu_{ss}$ were consistent with those previously measured in basaltic **(Violay et al., 2014)** and carbonate-bearing rocks **(Han et al., 2007; 2010; Violay et al., 2013)**. Comparing room-humidity and drained experiments shows that water had almost no effect on $\mu_p$ and $\mu_{ss}$ **(Figs. 2-4) (Violay et al., 2014**). However, for Etna basalt, experiments performed under undrained conditions **(Fig. 2)** had about 20% reduction of $\tau_{ss}$ compared to room-humidity and drained experiments. Moreover, the fluid pressure increased with slip under undrained conditions, but was constant under drained conditions **(Fig. 2)**. This is further supported by a temperature increase of 35ºC measured by the thermocouple immersed in the fluid of undrained experiments **(Fig. 5),** and < 5ºC in drained experiments (for $\sigma_n^{eff}(t_0)$ = 20 MPa, $\delta$ = 6 m and $V$ = 3 ms$^{-1}$). The undrained thermal pressurization coefficient defined as the pore pressure increase for a unit temperature increase ranges from 0.01 MPa/°C to 0.1 MPa/°C **(Ghabezloo and Sulem, 2009).** An increase in bulk temperature of 35ºC of the fluid results in an increase in pore pressure of 0.35–3.5 MPa. We interpret the reduction of $\tau_{ss}$ to result from TMP within the slipping zone. The measured shear stress reduction is consistent with the melt lubrication model of **Nielsen et al. (2008)** according to which the rate of extrusion of friction melt from the slipping zone is regulated by the difference between the viscous pressure of the melt and the normal stress acting on the fault. Although the Terzaghi's principle cannot be applied under melt-lubricated conditions, we may draw a parallel about the role of the effective normal stress: the increase in fluid pore pressure in the slipping zone limits the melt extrusion rate from the slipping zone in the same way as the decrease of the normal stress acting on the fault. In both cases, the bulk result is the reduction of the viscous shear stress. This is confirmed by the sample shortening rate lower under undrained (e.g., 0.089 mm/m) than drained (0.17 mm/m) conditions **(Fig. 2A and Table 1)**. Under undrained conditions, after the slip stopped, part of the pressurization $dP$ in excess of $P_f(t_0)$gradually decreased **(Fig. 2A)**. This indicates that *thermal* pressurization due to water thermal expansion during frictional heating was dropping upon cooling of the water (by conduction through the vessel metal. A residual *mechanical* pressurization endured after cooling, due to the permanent volume reduction in connection to sample shortening. The fluid in the inner chamber of the hollow cylindrical rock specimen is hydraulically isolated from the external chamber which was directly connected to the pressurizing system (**Suppl. Material S1**). During sample shortening, the fluid trapped in the central hallow of the specimen may exert spurious fluid pressures. However, the contribution of fluid pressure from the inner hollow was negligible during the experiments. In fact:

1) in Carrara marble, the Terzaghi's principle was satisfied assuming the imposed fluid pressure is the fluid pressure measured on the annular sample (**Violay et al., 2013**);

2) in basalt, the sample shortens faster in drained (e.g., s926) than in undrained (e.g., s925) conditions (**Fig. 2A**). As a consequence, experiments performed under drained conditions would result in larger reduction of the volume of the inner chamber and, being the inner

chamber hydraulically isolated, in higher (spurious) pore pressures. The bulk effect would be a lower measured shear stress in drained conditions than in undrained conditions, which is the opposite of what we measured ($\tau_{ss}$ is lower under undrained conditions, **Fig. 2A**); 3) similar experiments performed on solid cylinders (i.e., without the central hollow chamber) of gabbro under drained and undrained conditions resulted in $\tau_{ss}$ lower under undrained than drained conditions, confirming results obtained with hollow specimens (**Suppl. Material S2**).

As a consequence the effect of the fluid pressure from the inner chamber ( central hallow) on the axial load is negligible, and the axial cavity does not count as part of the simulated fault area. Indeed, all experimental results (e.g. peak friction value) are consistent with an effective normal stress ($\sigma_n$-$\alpha$ $P_f$) where the normal stress $\sigma_n$ is axial force normalized by the annular slip area only (e.g., **Violay et al., 2013; 2014**). The small to negligible contribution in fluid pressure during axial shortening from the fluid trapped in the inner hollow is due its epoxy filling. Epoxy is compliant and deforms during sampling shortening, buffering the increase in fluid pressure in the cavity.

In spite of the evidence of a measurable TMP, we question whether it is an efficient fault weakening mechanism during seismic slip, in particular in the presence of more rapid and effective alternative mechanisms. Under undrained conditions, fluid overpressures of ~1 MPa and 0.05 MPa were measured after 5 cm of slip for Etna basalt and Carrara marble, respectively (**Figs. 2A-B; 3A**). The initial overpressure ($dP$) was associated to a relative ($dP$ *100/$\tau_p$) apparent shear stress drop of maximum 10% for $\sigma_n^{eff}(t_0)$=20 MPa in Etna basalt (squared dots in **Fig. 4**), and no shear stress drop in Carrara Marble. Since the shear stress drop was 65-80% after 5 cm of slip for both lithologies, more efficient lubricating mechanisms may have been activated at the initiation of slip and at steady-state. Elasto-hydrodynamic lubrication or weakening induced by the overpressure generated by the shear of a thin viscous fluid comprised between two sub-parallel and rough surfaces (**Brodsky and**

**Kanamori, 2001**) may be excluded, as discussed in **Violay et al. (2013**). Cavitation or the formation of vapour-filled cavities in a flowing liquid due to rapid changes in pressure may also be excluded. When cavities implode, they produce intense fluid pressure variations that induce accelerated erosion of the solid surface and high levels of noise. However, there is (1) no evidence of abrupt variations in fluid pressure or normal stress in both drained and undrained conditions (see **Figs. 2 and 3A**) and (2) no intensification of surface erosion (wear) in experiments performed with fluids with respect to room-humidity (**Fig. 3B**). Moreover, acoustic emissions were recorded in experiments conducted with SHIVA but on Westerly granite in room-humidity and drained conditions (**Passelegue et al., 2013**). Noteworthy, the intensity and number of acoustic emissions increased in room-humidity conditions (i.e., in the absence of liquid water) suggesting that cavitation did not occur in the presence of pore fluids.

At the initiation of slip in both marble and basalt, the negligible contribution of TMP to the large frictional weakening of the experimental fault is further supported by the absence of variations in either normal stress or shortening (i.e. no evidence of dilatation) (**Fig. 3B**).

At steady-state, the ineffectiveness of TMP is demonstrated by **1)** the occurrence of solidified friction melts, which cover the surface of Etna Basalt cylinders independently of the fluid content. The experimental and microstructural observations suggest that the dominant weakening mechanism was flash heating causing melting at asperity contacts at the initiation of slip and frictional melt lubrication at steady-state **(Goldsby and Tullis, 2011, Brown and Fialko, 2012, Violay et al., 2014)** and **2)** the occurrence of ultrafine-grained material in water for Carrara marble experiments, independently of the hydraulic conditions. The experimental and microanalytical observations suggest that the dominant weakening mechanism in Carrara marble was probably flash heating of asperities at the initiation of sliding **(Violay et al., 2013, Spagnuolo et al., subm.)** or a grain-size (possibly water-enhanced) dependent process (superplasticity) at steady-state **(Verberne et al., 2014; Green et al., 2015; De Paola et al., in press.).**

At the initiation of sliding, the apparently small contribution of measured TMP to fault weakening under drained and undrained conditions might be partly due to the experimental configuration. Indeed, at short time intervals, heating affects only the water volume trapped in the slipping zone ($Vol_s$ ~2 $10^{-7}$ $m^3$, given the average thickness of ~0.16 mm induced by sample roughness over the 1.25 $10^{-3}$ $m^2$ of slipping area), which is small compared to the fluid volume in the vessel ($Vol_v$~5 $10^{-6}$ $m^3$). For reasonable fault-parallel permeability the water on the slipping zone and in the vessel are connected and pressure is at equilibrium. Then the volume expansion of heated slip-zone water:

$$dVol_{exp} = \lambda \Delta T \, Vol_s \qquad \text{Eq. 1}$$

is accommodated by the total water volume (λ being the water coefficient of thermal expansion). Assuming roughly constant λ, K (water incompressibility) and total available volume $Vol_s$+$Vol_v$ (i.e., neglecting volume changes due to compliance of the vessel or of rocks on natural faults), we obtain an upper bound pressurization reached during fault slip:

$$dP = K \, dVol_{exp}/(Vol_s+Vol_v) = K \, \lambda \, \Delta T \, Vol_s/(Vol_s+Vol_v) \qquad \text{Eq. 2}$$

On actual faults the volume of connected water (equivalent to $Vol_v$) per unit fault surface may be smaller than in the experiment, a condition which is readily extrapolated by reducing $Vol_v$ in equation (1). In order to estimate the maximum contribution of TMP to frictional weakening, we assume $Vol_v$ close to zero. The upper bound for pressurization is thus obtained assuming that (1) the heat produced by frictional sliding is entirely dissipated in a small water volume trapped in the slipping zone ($Vol_s$), (2) volume changes due to compliance of the vessel or of rocks on natural faults are negligible and (3) the buffering effect of thermal expansion of water by the connected volume is reduced to zero. Using λ=207 $10^{-6}$ ºC$^{-1}$, K= 2.1 GPa **(Waples and Waples, 2004),** $Vol_v$=0 and an estimated temperature increase of 20ºC after a slip of 0.1 m we obtain a maximum pressurization of ~1.1 MPa. The bulk temperature increase in the slipping zone (for $\tau(t) = \mu(t)\ (\sigma_n(t) - P_f(t))$ was estimated using the heat rate production and solving the 1D diffusion problem (Carslaw and Jaeger, 1959) such that:

$$T(t) = \frac{1}{\rho \cdot Cp \cdot \sqrt{\kappa\pi}} \cdot \int_0^t \frac{1}{2} \cdot \frac{\tau(t') \cdot V(t')}{\sqrt{t - t'}} dt \qquad \text{Eq. 3}$$

(where thermal capacity Cp = 880 J kg$^{-1}$ K$^{-1}$ and 116 J kg$^{-1}$ K$^{-1}$ respectively for calcite and basalt samples, density $\rho$ = 2700 kg m$^{-3}$ and 2900 kg m$^{-3}$ respectively for calcite and basalt sample and thermal diffusivity κ = 1.48 $10^{-6}$ m$^2$ s$^{-1}$ and 0.21 m$^2$ s$^{-1}$ respectively for calcite and basalt sample and *t* is the time need to slip from 0 and 100 mm (**Eppelbaum et al., 2014; Hanley et al., 1978; Waples and Waples, 2004;** for further details see **Violay et al., 2013).** From equations 2 and 3, the thermal pressurization of 1.1 MPa would induce a friction drop of about 15% from peak stress; such a drop was already achieved before 0.01 m of slip, even in drained or room-humidity experiments (**Fig. 3**). As a consequence, upon extrapolation to conditions where the water volume surrounding the fault is negligible, thermal pressurization is less efficient than other weakening mechanisms (e.g., flash weakening and heating of asperities) and would add a further relative weakening to an already lubricated fault. The contribution from thermal pressurization will decrease with increasing fluid connectivity and can be quantified as follows. From Eq. 2, the fluid volume expansion $dVol_{exp}$ due to the temperature increase results in an increase in pore fluid pressure:

$$P_{f(t)} = P_{f(t0)} + K \frac{\lambda\, \Delta T\, Vol_s}{Vol_v + Vol_s} \qquad \text{Eq. 4}$$

Weakening due to water pressurization $w_p$ increases with $P_f$:

$$w_p = \frac{\sigma_n - P_f(t)}{\sigma_n - P_{if(t0)}} \qquad \text{Eq. 5}$$

and is related to the connected fluid volume (in $m^3$) per unit fault surface in $m^2$. A value of $w_p = 1$ corresponds to no contribution to weakening from pressurized fluids (i.e., $P_f = P_f(t_0)$). From **Fig. 7**, the maximum effect of pressurization is a drop by 40% for connected volumes of less than a cubic centimetre per unit fault area (corresponding to $10^{-6}$ m). For values above 1 litre of connected water per unit fault area (corresponding to a water layer of average thickness 1 mm) the pressurization effect is buffered and negligible.

## Conclusions

We conclude that even extremely thin (< 100 µm) and low permeability (< $10^{-17}$ $m^2$ slipping zones, may lead to a relatively unimportant TMP of pore fluids during seismic slip. These new experimental results apply to slip surfaces within cohesive rocks where strain localization is instantaneous, resulting in rapid temperature increase of the slipping zone and leading to the activation of other weakening mechanisms **(Rice, 2006, Goldsby and Tullis, 2011, Di Toro et al., 2010).** In the case of non-cohesive rocks (gouges), strain is distributed within the gouge layer before being localized **(Beeler et al., 1996, Marone et al., 1990, Smith et al., 2015)**. These results in a gradual temperature increase during slip and TMP of pore fluids might still be an efficient fault weakening mechanism.

## References

Beeler N.M., et al., 1996. Frictional behavior of large displacement experimental faults. J. Geophys. Res., 101, 8697-8715

Bizzari, A. Cocco, M, 2006. A thermal pressurization model for the spontaneous dynamic rupture propagation on a three-dimensional fault: 1. Methodological approach. J. Geophys. Res., 111, B05303

Brantut, N., Schubnel, A., Rouzaud J.-N., Brunet F., Shimamoto T., 2008. High-velocity frictional properties of a clay bearing fault gouge and implications for earthquake mechanics, J. Geophys. Res., 113, B10401.

Brantut, N. et al., 2010. Thermochemical pressurization of faults during coseismic slip, J. Geophys. Res., 115, B05314

Brodsky, E.E., Kanamori, H., 2001. Elastohydrodynamic lubrication of faults. J. Geophys. Res. 106, 16357–16374.

Brown K. M., Fialko Y., 2012. Melt welt' mechanism of extreme weakening of gabbro at seismic slip rates. Nature, 488, 638-41

De Paola, N., Hirose, T. Mitchell, G. Di Toro, C. Viti, and T. Shimamoto (2011), Fault lubrication and earthquake propagation in thermally unstable rocks, Geology, 39, 35–38.

De Paola, N., Holdsworth, R.E., Viti, C., Collettini, C., Bullock, R. Can grain size sensitive flow lubricate faults during the initial stages of earthquake propagation, submitted to Earth and Planetary Science Letters.

Di Toro G. et al., 2010. From field geology to earthquake simulation: a new state-of-the-art tool to investigate rock friction during the seismic cycle (SHIVA). Rendiconti Lincei, 21, 95–114

Di Toro G. et al., 2011. Fault lubrication during earthquakes. Nature, 471, 494-498.

Eppelbaum L. et al., Applied Geothermics, Lecture Notes in Earth System Sciences, DOI: 10.1007/978-3-642-34023-9_2 Springer-Verlag Berlin Heidelberg 2014

Faulkner D.R., Mitchell T.M., Behnsen J., Hirose T., Shimamoto T. 2011 Stuck in the mud? Earthquake nucleation and propagation through accretionary forearcs Geophysical Research Letters, 38.

Ferri F., et al., 2010. Evidences of thermal pressurization in high velocity friction experiments on smectite-rich gouges Terra Nova, 22, 347–353

Fujiwara T. et al., 2011. The 2011 Tohoku-Oki Earthquake: Displacement Reaching the Trench Axis. Science, 334, 1240-1240

Ghabezloo S., Sulem J., 2009. Temperature induced pore fluid pressurization in geomaterials Rock Mech Rock Eng, 29-43

Goldsby D.L., Tullis T.E. 2011. Flash heating leads to low frictional strength of crustal rocks at earthquake slip rates. Science, 334, 216-218.

Green, H.W., Shi, F., Bozhilov, K., Xia, G., Reches, Z., 2015. Phase transformation and nanometric flow cause extreme weakening during fault slip. Nature Geoscience, DOI:10.1038/NGEO02436

Han R. Hirose, T., Shimamoto T., 2010. Strong velocity weakening and powder lubrication of simulated carbonate faults at seismic slip rates. J. Geophys. Res. 115, B03412

Han R., et al., 2007. Ultralow friction of carbonate faults caused by thermal decomposition, Science. 316, 878–881

Hanley, E.J., Dewitt, D.P., Roy, R.F., 1978. The thermal diffusivity of eight well characterized rocks for the temperature range 300–1000 K. Eng. Geol. 12, 31–47.

Hirose T, Shimamoto T., 2005. Growth of molten zone as a mechanism of slip weakening of simulated faults in gabbro during frictional melting. J. Geophys. Res., 110, B05202

Lachenbruch, A.H., 1980. Frictional heating, fluid pressure, and the resistance to fault motion. J. Geophys. Res., 85, 6097–6122.

Marone C., Raleigh C.B., Scholz C.H., 1990. Frictional behavior and constitutive modeling of simulated fault gouge. J. Geophys. Res., 95, 7007-7025

Mitchell T.M., Smith S.A.F., Anders M.H., Di Toro G., Nielsen S., Cavallo A., Beard A.D. 2015. Catastrophic emplacement of giant landslides aided by thermal decomposition: Heart Mountain, Wyoming Earth Planet. Sci. Lett., 411, 199–207.

Mizoguchi, K., Hirose, T., Shimamoto, T. and Fukuyama, E., 2009. High-velocity frictional behavior and microstructure evolution of fault gouge obtained from Nojima fault, southwest Japan. Tectonophysics, 471, 285–296

Nielsen, S. et al., 2008. Frictional melt and seismic slip. J. Geophys. Res., 113, B01308.

Niemeijer, A. et al., 2011. Frictional melting of gabbro under extreme experimental conditions of normal stress, acceleration, and sliding velocity. J. Geophys. Res., 116, B07404.

Passelègue F.X., Spagnuolo, E., Violay, M., Nielsen, S.B., Di Toro, G., Schubnel, A., 2013. Influence of slip rate and normal stress on off-fault damage in high-velocity friction experiments on crustal rocks. , American Geophysical Union Annual Meeting Abstracts with Programme T33C-2651.

Paterson, M. S., Wong T.-F., (2005). The brittle field, Second ed., 347, Springer Verlag, Berlin, New York.

Platt J. D., Rudnicki J. W., Rice J. R., 2014. Stability and Localization of Rapid Shear in Fluid-Saturated Fault Gouge, 2. Localized zone width and strength evolution, J. Geophys. Res., 119, 4334-4359

Reches, Z, Lockner D.A., Fault weakening and earthquake instability by powder lubrication. Nature, 467, 452-455

Rice J.R., 2006. Heating and weakening of faults during earthquake slip. J. Geophys. Res, 111, B05311

Rice JR., 1992. Fault stress states, pore pressure distributions, and the weakness of the San Andreas Fault. In Fault Mechanics and Transport Properties of Rocks, ed. B Evans, Tf Wong, pp. 475–504. London: Academic.

Segall, P. & Rice, J.R., 2006. Does shear heating of pore fluid contribute to earthquake nucleation? J. geophys. Res., 111, B09316

Sibson R.H., 1973. Interactions between Temperature and Pore-Fluid Pressure during Earthquake Faulting and a Mechanism for Partial or Total Stress Relief, Nature, 243, 66–68

Smith S.A.F. Nielsen S., Di Toro G. 2015. Strain localization and the onset of dynamic weakening in calcite fault gouge. Earth Planet. Sci. Lett., 413, 25-36

Tsutsumi A., Shimamoto T., 1997. High-velocity frictional properties of gabbro. Geophys. Res. Lett., 24, 699–702

Ujiie K., Tsutsumi A., Kameda J.2011. Reproduction of thermal pressurization and fluidization of clay-rich fault gouges by high-velocity friction experiments and implications for seismic slip in natural faults Rick Sibson, Geological Society of London Special Publication, 359, 267–285

Ujiie, K., *et al.* 2013, Low coseismic shear stress on the Tohoku-oki megathrust determined from laboratory experiments, Science, 342, 1211–1214.

Verberne B.A, et al., 2014. Superplastic nanofibrous slip zones control seismogenic fault friction Science. 346, 1342-1344.

Vinciguerra S., et al., 2005. Relating seismic velocities, thermal cracking and permeability in Mt. Etna and Iceland basalts J. Rock Mech., 42900-42910.

Violay M. et al., 2012. Pore fluid in experimental calcite-bearing faults: abrupt weakening and geochemical signature of co-seismic processes. Earth Planet. Sci. Lett. 361, 74–84

Violay M. et al., 2014. Effect of glass on the frictional behavior of basalts at seismic slip rates, Geophys. Res. Lett. 41, 348-355

Violay M. et al., 2014. Effect of water on the frictional behavior of cohesive rocks during earthquakes. Geology. 42, 27-30

Waples, D.W., Waples, J.S., 2004. A review and evaluation of specific heat capacities of rocks, minerals, and subsurface fluids. Part 1: Minerals and nonporous rocks. Nat. Resour. Res. 13 , 13–130.

Wibberley, C.A.J. Shimamoto T, 2005. Earthquake slip weakening and asperities explained by thermal pressurization. Nature, 436, 689–692.

## ACKNOWLEDGMENTS

We thank R. Lüchinger (ETH) for thin sections preparation and P. Scarlato (INGV), and E. Reusser (ETH) for laboratory support. We acknowledge S. Vinciguerra and R. Bakker for their help with the experiments. MV and JPB thank the ETH and GDT, SN and ES the ERC grant No 614705 NOFEAR for the financial support.

**FIGURES CAPTIONS:**

**Figure. 1:** Friction coefficient versus slip in Etna basalt. Experiments were performed at slip rate, $V$ = 3 ms$^{-1}$ (target slip rate), acceleration = 7.8 ms$^{-2}$, and initial normal stress ($\sigma_n^{eff}(t_0)$) comprised between 10 MPa and 30 MPa under either drained conditions (experiments s928, s926 and s930), and undrained conditions (s932, s922, and s924). Independently of the initial $\sigma_n^{eff}(t_0)$, a reduction of ~20% of $\mu_{ss}$ was measured in the experiments performed under undrained conditions. The regular oscillations (~0.125 m in wavelength) in shear stress in the initial 3-4 meters of slip observed in experiment s932 are interpreted as due to the not perfect alignment of the sheared samples. In fact, the wavelength of the oscillations corresponds to the equivalent sample circumference [$\pi$ ($r_{external}$ + $r_{internal}$) = 0.1256 m]. The amplitude of the oscillations decreases progressively with cumulated slip due to wear and melting of the sliding surfaces and disappears after 4 m of slip.

**Figure 2:** Shear stress versus slip in Etna basalt and Carrara marble. Experiments were performed at $V$ = 3 ms$^{-1}$ (target slip rate), acceleration = 7.8 ms$^{-2}$, and initial effective normal stress ($\sigma_n^{eff}(t_0)$) = *20 MPa* at the initiation of the experiments under following environmental and hydraulic conditions: A) Etna basalt: room-humidity (s485 $\sigma_n$= 20 MPa: black curve), pore water under drained conditions (s921 and s926: red and green curve), pore water under undrained conditions (s922, s925, s927 and s933: yellow, orange, purple, and blue curves). B) Carrara marble: room-humidity (s307 $\sigma_n$= 20 MPa: black curve), pore water under drained conditions (s1023 and s1035: red and green curve), pore water under undrained conditions (s1024 and s1028: yellow and blue curves). Pore water pressure (full line) and shortening (dashed line) for drained and undrained experiments are depicted with the same colors as the reported shear stress.

**Figure 3:** Mechanical data. A) Close up of the first 0.05 m of slip of Fig. 1A for experiments s485 (room-humidity, black curve), s922, s933 (drained, purple and blue curves), s921, s926, (undrained, red and green curves). Pore water pressure for drained and undrained experiments are depicted with the same colors as the reported shear stress. B) Normal effective stress and shortening versus slip plot for experiments s485 (room-humidity, black curve), s922, s933 (drained, purple and blue curves), s921 and s926 (undrained, red and green curves).

**Figure 4:** Summary figure of the mechanical data for Etna basalt (22 experiments, Figs. A and B) and Carrara marble (11 experiments, Figs. C and D) reported in this study. Experiments were performed at $V = 3$ ms$^{-1}$ (target slip rate), acceleration = 7.8 ms$^{-2}$, and $P_f(t_0)$ ~5 MPa at the initiation of the drained and undrained experiments. A) Etna basalt: - friction coefficient vs. effective normal stress with respect to the pore fluid pressure at steady-state ($\sigma_n^{eff}(t)=\sigma_n(t) - (P_f(t_0) + dP)$), i.e. total fluid pressure, including variations due to fluid heating and mechanical effects of sample shortening and volume change in the vessel) under room-humidity conditions (green circles), drained conditions (red circles) and undrained conditions. - Blue squares: Friction coefficient vs. effective normal stress with respect to the pore fluid pressure at the initiation of the experiment ($\sigma_n^{eff\text{-}0}(t)=\sigma_n(t) - P_f(t_0)$. The steady-state shear stress data normalized by the normal effective stress at $t_0$ show a systematic decrease of c. 20% with respect to the steady-state shear stress normalized by the effective stress at steady-state. Therfore, the double faced black arrows highlights the role of thermo-mechanical pressurization.

B) Etna basalts: percentage of residual friction with respect to the steady-state friction after 5 cm of slip vs. effective normal stress under room-humidity conditions (green circles) drained conditions (red circles) and undrained conditions (blue circles). Y axis: $\mu_p$= peak friction, $\mu_{ss}$ = steady-state friction, $\mu_r$ = residual friction. (C) and (D), case for Carrara Marble. Standard deviation is within the dimension of the symbols.

**Figure 5:** Evolution of the shear stress (blue curve) and temperature (red curve) measured by the thermocouple during experiment s929 (undrained conditions).

**Figure 6:** Slipping zones of Etna basalt after steady-state friction was achieved (>1 m of slip). Experimental conditions: acceleration 7.8 $ms^{-2}$, initial $\sigma_n^{eff}(to)$= 20 MPa and slip rate, $V$ = 3 $ms^{-1}$. A-B: Room-humidity conditions C-D: Drained conditions. E-F: Undrained conditions. Independently of the environmental conditions, at the end of experiments, the wall rocks were separated by continuous layer of glass. B, D and F are enlargements of the slipping zones. Field emission scanning electron microscope- Backscattered electron images.

**Figure 7:** Weakening due to water pressurization $w_p$ versus the connected volume per unit fault surface (values of $w_p = 1$ correspond to no weakening). Maximum effect of pressurization is a drop to 40% for connected volumes of less than a cubic centimeter per unit fault area. For values above 1 liter of connected buffering water, the pressurization effect is negligible.

**Table 1:** Summary of experimental conditions and results. See main text for explanations. C.M. = Carrara marble; E.B.=Etna basalt.

**Table 2:** Chemical composition of the basalt and of the glass. Chemical bulk composition of the Etna basalt (Giordano and Dingwell, 2003*); Electron MicroProbe Analysis (EMPA) chemical compositions of the initial glass and of the solidified frictional melt. The EPMA analysis do not close to about 100% because only Fe2+ was determined. The S.D. refers to the standard deviation of the EMPA composition of the solidified friction melts.

* Giordano and Dingwell. 2003. Viscosity of hydrous Etna basalt: implications for plinian-style basaltic eruptions. bull Volcanol 65:8-14.

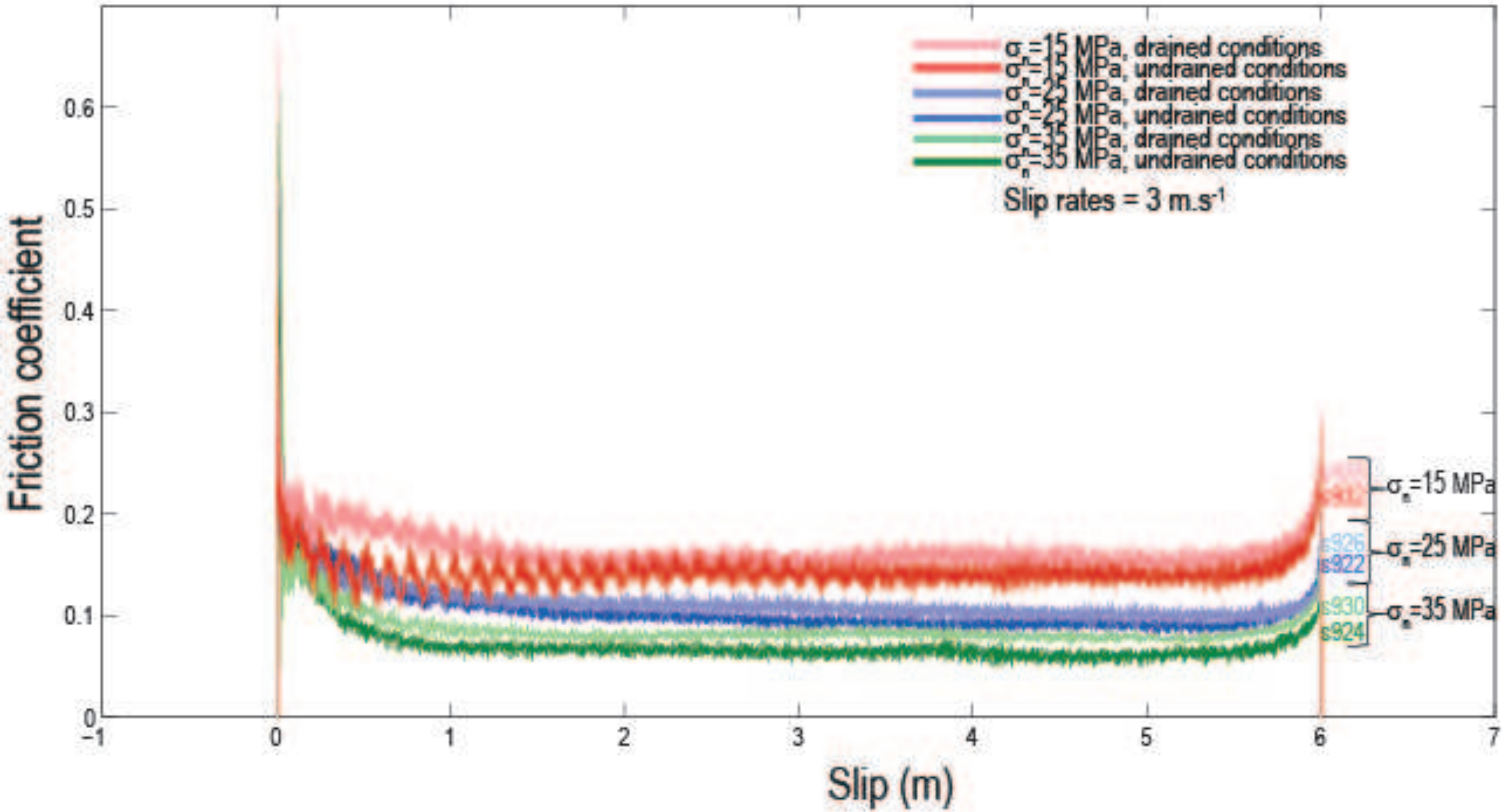

σn=15 MPa, drained conditions
σn=15 MPa, undrained conditions
σn=25 MPa, drained conditions
σn=25 MPa, undrained conditions
σn=35 MPa, drained conditions
σn=35 MPa, undrained conditions
Slip rates = 3 m.s-1
σn=15 MPa
s926
s922
σn=25 MPa
s930
s924
σn=35 MPa
Friction coefficient
Slip (m)
0
0.1
0.2
0.3
0.4
0.5
0.6
−1
0
1
2
3
4
5
6
7

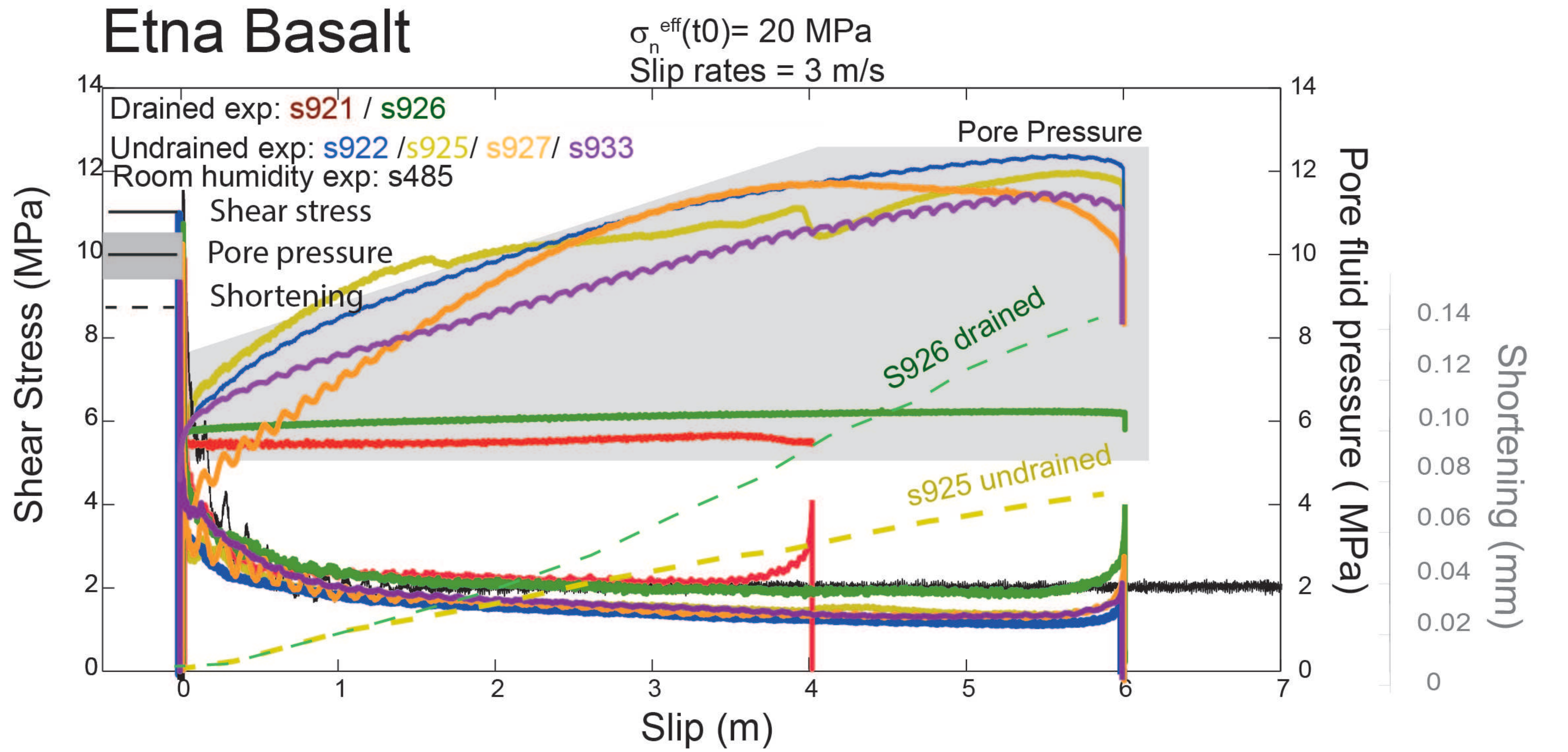

Etna Basalt
$\sigma_n^{eff}$(t0)= 20 MPa
Slip rates = 3 m/s
Drained exp: s921 / s926
Undrained exp: s922 /s925/ s927/ s933
Room humidity exp: s485
Shear stress
Pore pressure
Shortening
Pore Pressure
S926 drained
s925 undrained
Shear Stress (MPa)
Pore fluid pressure ( MPa)
Shortening (mm)
Slip (m)


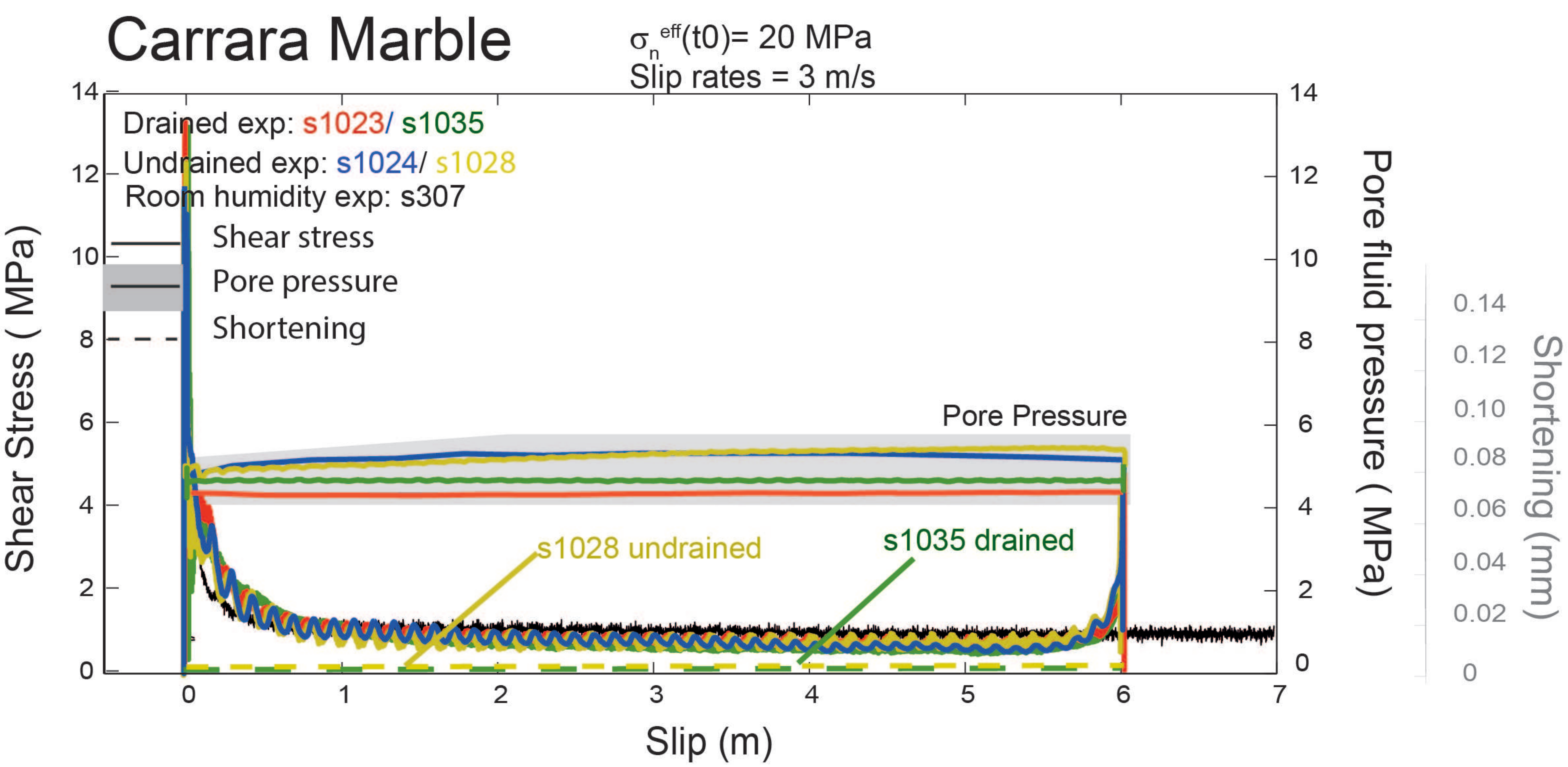

Carrara Marble
$\sigma_n^{eff}$(t0)= 20 MPa
Slip rates = 3 m/s
Drained exp: s1023/ s1035
Undrained exp: s1024/ s1028
Room humidity exp: s307
Shear stress
Pore pressure
Shortening
Pore Pressure
s1028 undrained
s1035 drained
Shear Stress ( MPa)
Pore fluid pressure ( MPa)
Shortening (mm)
Slip (m)

A) Close up of the first 5 cm of slip in Fig.2a
σn eff(t0)= 20 MPa
Slip rates = 3 m/s
Room humidity exp: s485
Drained exp: s921 / s926
Undrained exp: s922 / s933
Pf_s922
Pf_s933
Pf_s926
Pf_s921
Shear Stress (MPa)
Pore fluid pressure ( MPa)
Slip (m)
B)
Shortenning
Normal stress
σ_s933
σ_s921
σ_s926
σ_s922
σ_s485
Shortening (mm)
Normal stress (MPa)
Slip (m)

Etna basalt
A)
B)
Carrara marble
C)
D)
Peak friction
Steady-state friction
TMP
Friction Coefficient/
Normalized shear stress
Friction drop at 5 cm slip (%)
Initial effective normal stress (MPa)
μss Drained conditions
μss Room humidity conditions
μss Undrained conditions(τss/σeffss)
Normalized shear stress
Undrained conditions ( τss/σeff at t0)

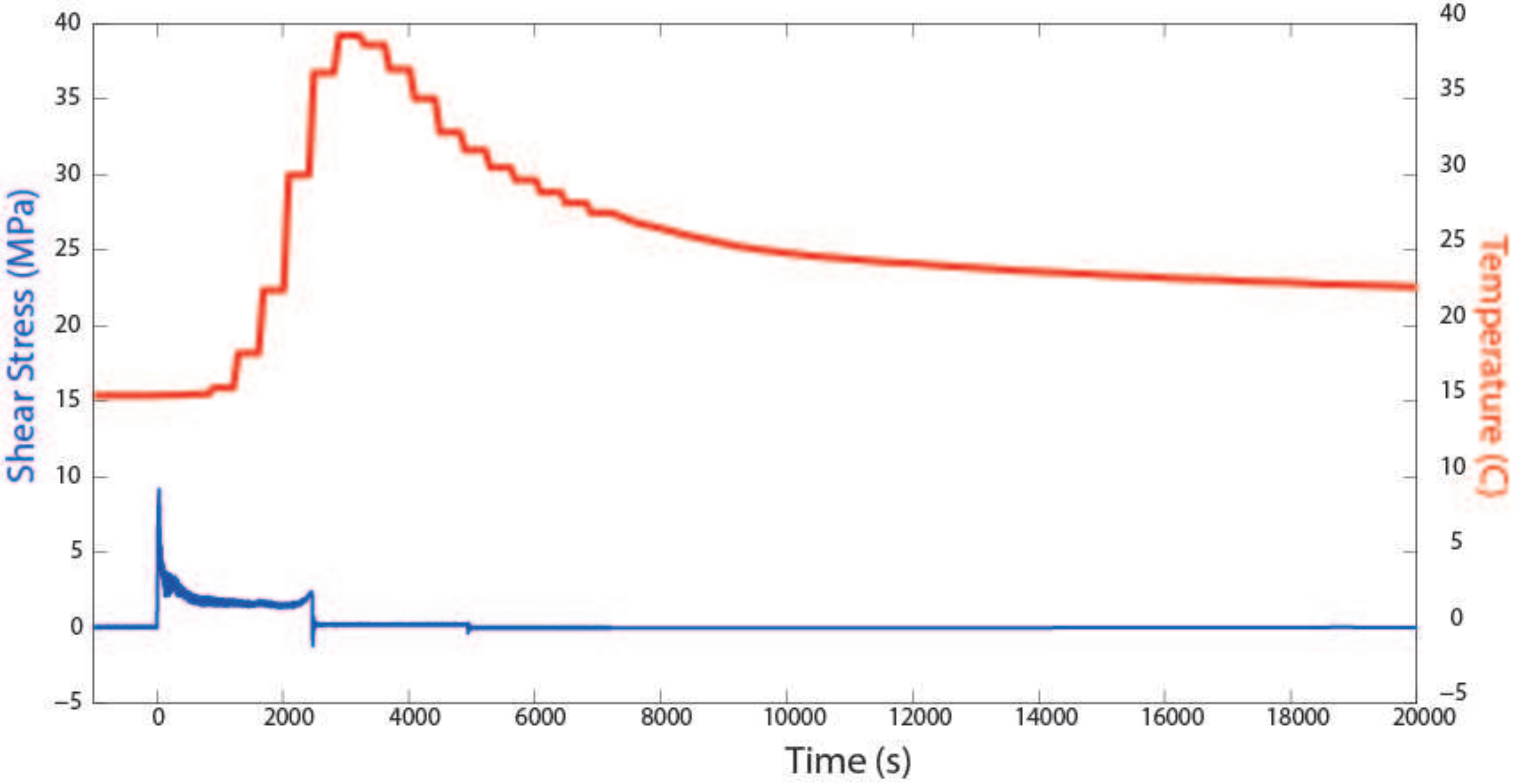

Shear Stress (MPa)
Temperature (C)
Time (s)
40
35
30
25
20
15
10
5
0
−5
0
2000
4000
6000
8000
10000
12000
14000
16000
18000
20000

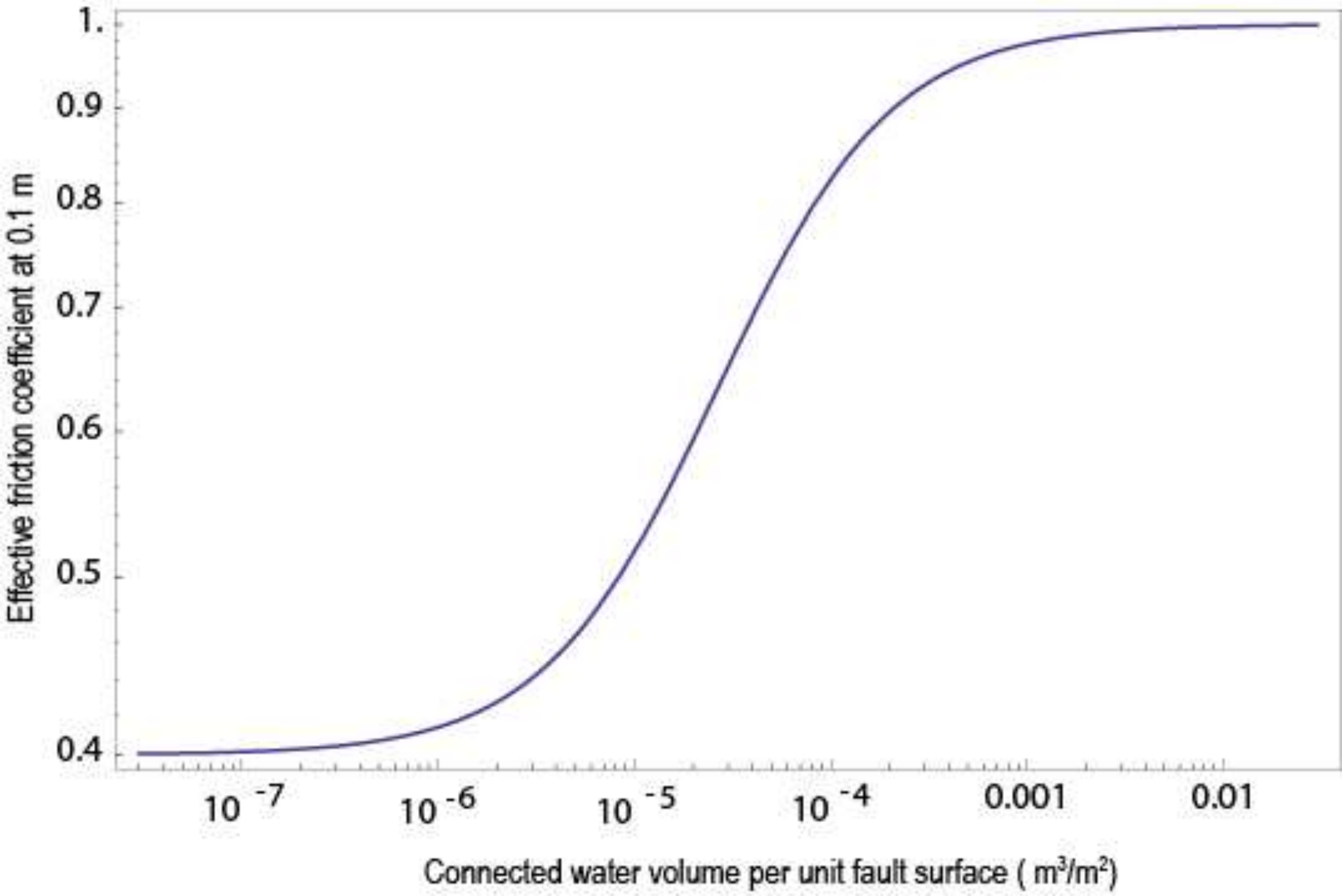

Effective friction coefficient at 0.1 m
1.
0.9
0.8
0.7
0.6
0.5
0.4
10 -7
10 -6
10 -5
10 -4
0.001
0.01
Connected water volume per unit fault surface ( m3/m2)